Available online at www.sciencedirect.com
SCIENCE DIRECT®
Journal of Sound and Vibration 279 (2005) 955–967
JOURNAL OF SOUND AND VIBRATION
www.elsevier.com/locate/jsvi

Impact dampers for controlling chaos in systems with limited power supply

S.L.T. de Souza[a], I.L. Caldas[a], R.L. Viana[b,*], J.M. Balthazar[c], R.M.L.R.F. Brasil[d]

[a] *Instituto de Física, Universidade de São Paulo, C.P. 66318, 05315-970 São Paulo, SP, Brazil*
[b] *Departamento de Física, Universidade Federal do Paraná, C.P. 19081, 81531-990 Curitiba, Brazil*
[c] *Departamento de Estatística, Matemática Aplicada e Computacional, Instituto de Geociências e Ciências Exatas, Universidade Estadual Paulista, 13500-230 Rio Claro, SP, Brazil*
[d] *Departmento de Engenharia Estrutural e de Fundações, Escola Politécnica, Universidade de São Paulo, 05424-930 São Paulo, SP, Brazil*

Received 3 July 2003; accepted 25 November 2003

Abstract

We investigate numerically the dynamical behavior of a non-ideal mechanical system consisting of a vibrating cart containing a particle which can oscillate back and forth colliding with walls carved in the cart. This system represents an impact damper for controlling high-amplitude vibrations and chaotic motion. The motion of the cart is induced by an in-board non-ideal motor driving an unbalanced rotor. We study the phase space of the cart and the bouncing particle, in particular the intertwined smooth and fractal basin boundary structure. The control of the chaotic motion of the cart due to the particle impacts is also investigated. Our numerical results suggests that impact dampers of small masses are effective to suppress chaos, but they also increase the final-state sensitivity of the system in its phase space.

1. Introduction

Vibro-impact systems have oscillating parts colliding with other vibrating components or rigid walls [1–5]. A vibro-impact system of practical importance is an impact damper, where the vibration of a primary system is controlled by the momentum transfer through collisions of the primary system with a secondary loose mass which bounces back and forth [6]. Impact dampers have been used to control high-amplitude oscillations, such as those typically appearing in chaotic motion, and hence these vibro-impact systems can be regarded as devices for controlling chaos in

*Corresponding author.
E-mail address: viana@fisica.ufpr.br (R.L. Viana).

0022-460X/$ - see front matter © 2004 Elsevier Ltd. All rights reserved.
doi:10.1016/j.jsv.2003.11.068

mechanical engineering systems [7]. In fact, impact dampers have been used to perform such tasks in cutting tools [8], turbine blades [9], and chimneys [10].

In recent papers, Chaterjee and co-workers [6,7] have studied the dynamics of impact dampers for both externally and self-excited oscillators. Their model consists of a damped oscillating cart and a point mass which collides with walls carved on the cart. It is through these seemingly random collisions that the momentum transfer is effective to decrease the amplitude of oscillations, in particular for situations where the dynamics is chaotic, either of a transient or stationary nature. A simple (ideal) model supposes a periodic forcing coming from an external source which is not appreciably perturbed by the motion of the cart [11–13].

However, in practical situations the dynamics of the forcing system cannot be considered as given a priori, and it must be taken as also a consequence of the dynamics of the whole system [14]. In other words, the forcing system has a limited energy source, as that provided by an electric motor for example, and thus its own dynamics is influenced by that of the oscillating system being forced [15,16]. This increases the number of degrees of freedom, and is called a non-ideal problem. In terms of the vibrating cart model of Ref. [6], the non-ideal system is obtained by replacing the external sinusoidal driving of the cart by a rotor attached to the cart, and fed by a motor [14]. The angular momentum of the rotor is imparted to the cart. The application of the non-ideal model to the gear rattling dynamics has been done in a recent paper [17].

In this paper, we aim to analyze some dynamical aspects of the non-ideal problem in a general context of impact damper dynamics, putting emphasis on two features: (1) the attraction basin structure in phase space, and (2) the control of chaotic impacts caused by the addition of an impact damper to a non-ideal oscillator. The phase space structure of the dynamics of a vibro-impact system, as it occurs with forced non-linear systems in general, can be very complicated due to the coexistence of attractors with highly interwoven basins of attraction [18,19]. These basins are typically fractal [20] and exhibit final-state sensitivity: small uncertainties on specifying the initial conditions (in phase space) may lead to a great deal of uncertainty in the determination of what attractive stationary state the system will asymptote to for long times [21]. On the other hand, the control of chaotic motion has been a goal studied for more than a decade [22], and presents various technological challenges to be implemented in engineering systems [23]. Impact dampers were originally devised to control high-amplitude oscillations, but they can also have a chaos suppression effect.

This paper is organized as follows: Section 2 introduces the combined system of ordinary and algebraic equations describing the dynamics of a non-ideal system without impact dampers. Section 3 shows numerical results on the basin boundaries for this model, evidencing final-state sensitivity and an apparently fractal structure. The inclusion of the impact dampers, by means of a bouncing particle with momentum transfer to the vibrating cart, is left to Section 4, where the boundary conditions are worked out in order to yield numerical solutions for the equations of motion. Section 5 presents numerical results about controlling of chaotic motion of the cart by means of its interaction with the impact dampers, and the effect of the latter on the phase space structure. Our conclusions are left to the final section.

2. Non-ideal model without impacts

We will first consider the one-dimensional motion of a cart of mass M connected to a fixed frame by a non-linear spring and a linear viscous damper (damping coefficient c) (Fig. 1(a)). The

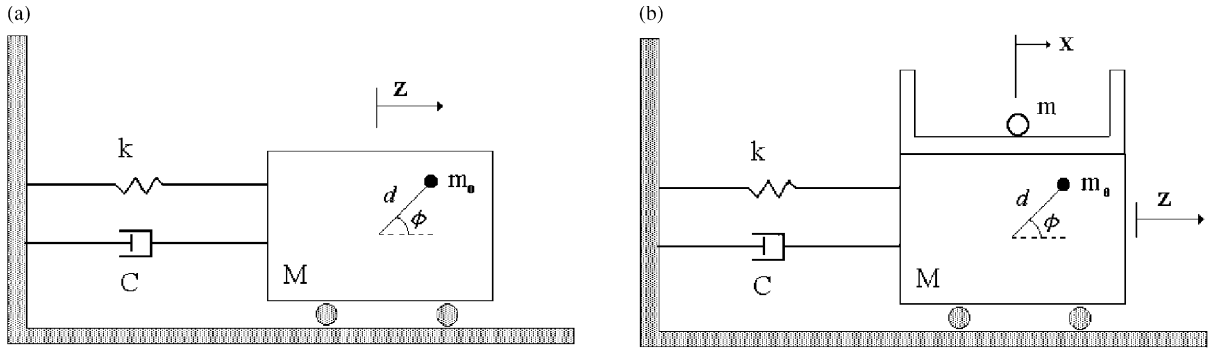

Fig. 1. (a) Schematic model of a cart oscillation driven by a rotor; (b) model with a bouncing particle.

non-linear spring stiffness is given by $k_1Z - k_2Z^3$, where Z denotes the cart displacement with respect to some equilibrium position in the absolute reference frame. The motion of the cart is due to an in-board non-ideal motor driving an unbalanced rotor with moment of inertia J. We denote by ϕ the angular displacement of the rotor, and model it as a particle of mass m_0 and radial distance d from the rotation axis.

This non-ideal problem has two-degrees-of-freedom, represented by the generalized co-ordinates Z and ϕ, and respective velocities $\dot{Z}$ and $\dot{\phi}$. The Euler–Lagrange equations of motion are

$$\frac{\mathrm{d}}{\mathrm{d}t}\left(\frac{\partial \mathscr{L}}{\partial \dot{Z}}\right) - \frac{\partial \mathscr{L}}{\partial Z} = -\frac{\partial \mathscr{F}}{\partial \dot{Z}}, \tag{1}$$

$$\frac{\mathrm{d}}{\mathrm{d}t}\left(\frac{\partial \mathscr{L}}{\partial \dot{\phi}}\right) - \frac{\partial \mathscr{L}}{\partial \phi} = -\frac{\partial \mathscr{F}}{\partial \dot{\phi}}, \tag{2}$$

where $\mathscr{L} = T - V$ is the Lagrangian function, and $\mathscr{F}$ is Rayleigh's dissipation function. The kinetic energy is

$$T(Z, \phi, \dot{Z}, \dot{\phi}) = \tfrac{1}{2}(M + m_0)\dot{Z}^2 + \tfrac{1}{2}J\dot{\phi}^2 - m_0 d\dot{\phi}^2 Z^2 \sin\phi, \tag{3}$$

whereas the potential energy and dissipation function are, respectively,

$$V(Z) = \tfrac{1}{4}k_2Z^4 - \tfrac{1}{2}k_1Z^2, \tag{4}$$

$$\mathscr{F}(\dot{Z}, \dot{\phi}) = \tfrac{1}{2}c\dot{Z}^2 - \tilde{E}_1\dot{\phi} + \tfrac{1}{2}\tilde{E}_2\dot{\phi}^2, \tag{5}$$

where $\tilde{E}_1$ and $\tilde{E}_2$ are damping coefficients for the rotor, which can be estimated from the characteristic curve of the energy source (a DC-motor) [14].

It is convenient to normalize the co-ordinates and time according to

$$Z \to z \equiv \frac{Z}{d}, \tag{6}$$

$$t \to \tau \equiv \sqrt{\frac{k_1}{M + m_0}}t = \sqrt{\frac{\varepsilon k_1}{m_0}}t, \tag{7}$$

where d is the rotor arm, and we introduced a "reduced mass"

$$\varepsilon \equiv \frac{m_0}{M + m_0} \tag{8}$$

which is typically a small dimensionless number, provided the mass of the rotor is much less than the mass of the cart.

In this way, the equations of motion resulting from substituting Eqs. (3)–(5) in Eqs. (1) and (2) can be written as

$$\ddot{z} + \mu\dot{z} - z + \delta z^3 = \varepsilon(\ddot{\phi}\sin\phi + \dot{\phi}^2\cos\phi), \tag{9}$$

$$\ddot{\phi} = \ddot{z}\sin\phi + E_1 - E_2\dot{\phi}, \tag{10}$$

where we have introduced the auxiliary quantities

$$\mu \equiv \frac{c}{\sqrt{k_1(M + m_0)}}, \quad \delta \equiv \frac{k_2}{k_1}d^2. \tag{11, 12}$$

3. Final-state sensitivity in the non-ideal system

The dynamics of the non-ideal system can be described by Eqs. (9) and (10). The motion of the cart itself can be viewed in a two-dimensional subspace of the full phase space, in which we plot the cart displacement versus velocity. Fig. 2(a) shows phase portraits in which there are two coexisting, apparently chaotic attractors, named as A and B. The phase trajectories will asymptote to either one, according to initial conditions. These attractors are located symmetrically with respect to the $z = 0$ and $\dot{z} = 0$ lines, thanks to the $z \to -z$ and $\dot{z} \to -\dot{z}$ symmetries possessed by Eqs. (3)–(5). Fig. 2(b) shows the basins of attraction corresponding to the attractors A and B of Fig. 2(a), represented as white and black regions, respectively. These regions show up as smooth lobes from which emanate striations which encircle the lobes such that there is a very fine scale structure.

This figure is reminiscent of the basin boundary structure displayed by a particle in a two-well potential [18]. In fact, the symmetry of the vector field with respect to $z = 0$ is shared by both systems. Moreover, the motion of the cart itself, putting aside the fact that it is just a part of a composite system including also a motor-driven rotor, is essentially of a damped and driven Duffing system, thanks to the non-linear stiffness adopted. Chaotic dynamics in these kinds of systems with impacts can be quantitatively characterized by means of the Lyapunov exponents [24]. For the chaotic attractors A and B it turns out that the maximal Lyapunov exponent is, in fact, a positive number (≈ 0.1 for both), as indicated by Figs. 2(c) and (d), respectively.

However, as it has been observed in systems like the kicked double rotor [25], there appear to be regions for which the basin boundary is smooth (like the central lobes shown in Fig. 2(b)) and regions where the basin boundary is fractal, both regions being intertwined in a very fine scale. In other words, there are non-fractal boundary segments arbitrarily close to any fractal boundary segment. The box-counting dimension of the fractal boundary pieces has been computed by using the uncertainty exponent algorithm [21].

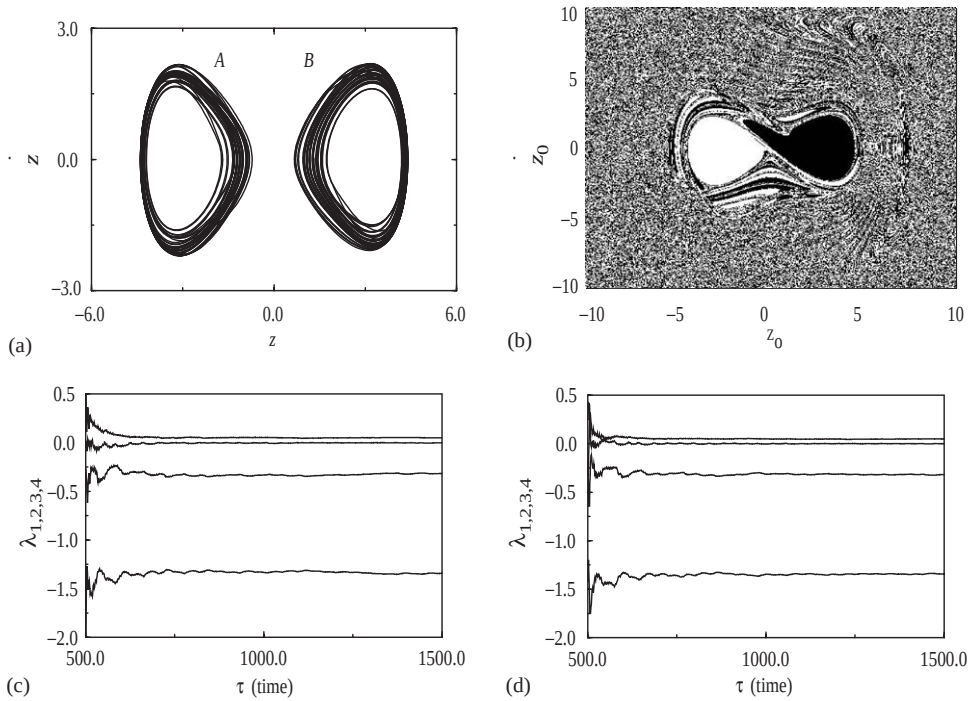

Fig. 2. (a) Displacement versus velocity of the cart, for $\mu = 0.02$, $\delta = 0.1$, $\varepsilon = 0.1$, $E_1 = 2.5$, $E_2 = 1.5$, and initial conditions $\phi_0 = \dot{\phi}_0 = 0$, showing two chaotic attractors named as A and B; (b) basins of attraction of the attractors A (white region) and B (dark region); Lyapunov exponents, as a function of the scaled time, for the attractor (c) A; (d) B.

Two small boxes from Fig. 2(b), and containing an apparently fractal part of the boundary, have been picked up (Figs. 3(a) and (b)). For both regions we have evaluated the relative number of initial conditions, belonging to these boxes, which are uncertain in the sense that a small deviation $\varpi \ll 1$ would render the evolution to be towards a different attractor from the original initial condition. It is expected that the uncertain fraction, or the area occupied by uncertain initial conditions, scales algebraically with the uncertainty $f(\alpha) \sim \varpi^{\alpha}$, where $\alpha = D - d_B$ is the uncertainty exponent, $D = 2$ is the phase space dimension, and d_B is the boundary box-counting dimension [20].

Fig. 3(c) shows a log–log plot of the uncertain fraction versus the radius of an uncertainty ball ϖ for the boxes depicted in Fig. 3(a) and (b). The points are fitted by straight lines, whose slopes are the corresponding uncertainty exponents, given by $\alpha = 0.38 \pm 0.02$ for box (a) and 0.40 ± 0.02 for box (b). Hence, it turns out that the box-counting dimension of the basin boundary, taking into account the similar results (up to the statistical uncertainty) for the two different boxes shown, is $d_B \approx 1.61$, resulting into a highly fractal structure, and a quantitative evidence of final-state sensitivity. For example, if we were to try a reduction on the uncertain fraction by decreasing the uncertainty radius ϖ by 50%, for example, the corresponding decrease in $f(\alpha)$ would be of just 24%. Thus, the fractal nature of the basin boundary results in a severe obstruction to determine what attractor will a given initial condition asymptote to, for it is always known within a given experimental error interval.

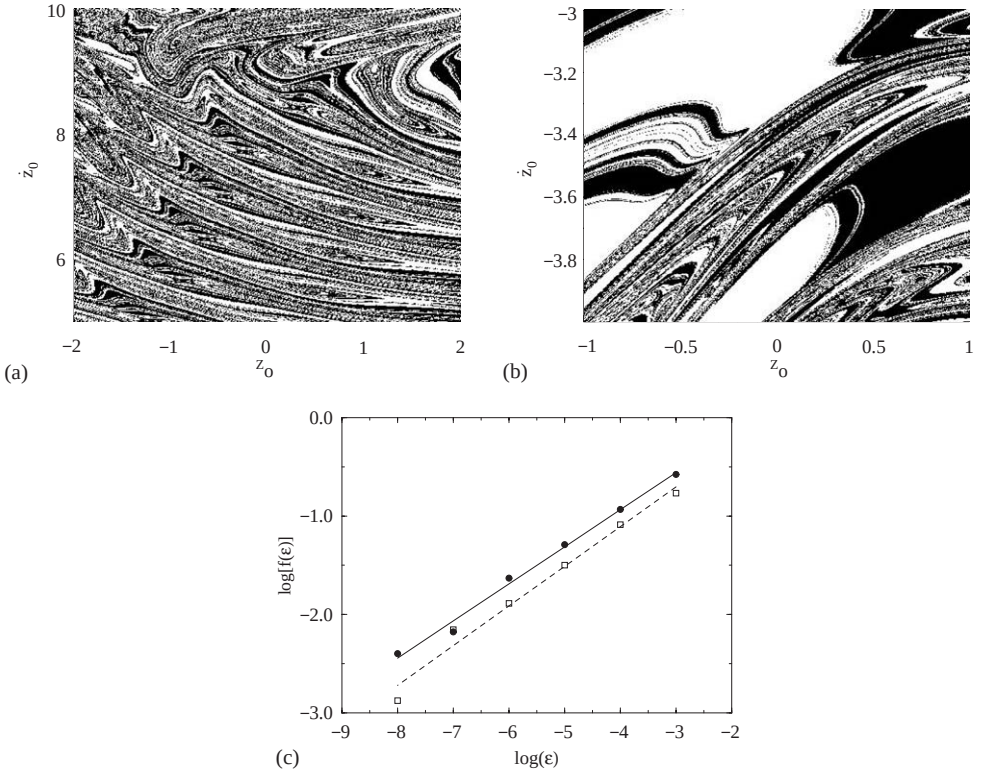

Fig. 3. (a) and (b) Two boxes picked up from Fig. 2(b) and which exhibits an apparently fractal basin structure; (c) uncertain fraction versus the radius of an uncertainty ball centered at an initial condition chosen from boxes (a—filled circles) and (b—open squares). The solid and dashed lines are least squares fits, respectively.

4. Non-ideal model with an impact damper

Now we consider the system with the impacts of a third mass, m, which is free to move back and forth between walls rigidly attached to the cart. These walls come from an impact damper consisting of a wide gap carved in the upper part of the cart (Fig. 1(b)). The mass of the impact damper will be absorbed into the total mass of the cart M. This introduced an additional degree of freedom to the above dynamical system, and accordingly we denote $X(t)$ the displacement of the point mass m, which is bounded by the moving walls. Between two successive impacts the motion is taken to be without friction, i.e., it is the solution of the simple differential equation, written in terms of $x \equiv X/d$:

$$\frac{\mathrm{d}^2 x}{\mathrm{d}\tau^2} = 0. \tag{13}$$

The initial conditions of this problem, $x(\tau_0) = x_0$ and $\dot{x}(\tau_0) = \dot{x}_0$, are determined by each impact of m with the movable boundaries, which are given by the solution of the cart motion [26]. Unlike the cart equations of motion (9) and (10), the particle equation (13) can be analytically solved

between two impacts, where the particle displacement and velocity are, respectively,

$$x(\tau) = x_0 + \dot{x}_0(\tau - \tau_0), \quad \dot{x}(\tau) = \dot{x}_0. \tag{14, 15}$$

On the other hand, an impact occurs wherever

$$x(\tau) = z(\tau) \pm \frac{v}{2}, \tag{16}$$

where v is the width of the damper gap existing above the cart (after being divided by d, for the sake of non-dimensionalization), and $z(\tau)$ is determined by solving the motion of the cart. In this case, we reset the initial conditions for the particle

$$\tau_0 = \tau, \quad x_0 = x(\tau), \quad z(\tau_0) = z(\tau) \tag{17–19}$$

and consider inelastic collisions, with a restitution coefficient $0 < r < 1$, so that, just after the impact we have

$$\dot{x}_0 = \dot{x}(\tau) - \sigma(1 + r)[\dot{x}(\tau) - \dot{z}(\tau)], \tag{20}$$

$$\dot{z}(\tau_0) = \dot{z}(\tau) + \sigma(1 + r)[\dot{x}(\tau) - \dot{z}(\tau)], \tag{21}$$

where a second reduced mass σ is defined for the particle–cart pair, such that

$$\frac{m}{M} = \frac{\sigma}{1 - \sigma}. \tag{22}$$

It will be convenient later to pass to a reference frame moving with the cart, so that the relative displacement of the particle is thus $y(\tau) = x(\tau) - z(\tau)$. In this relative frame, the particle solutions (14) and (15) become

$$y(\tau) = y_0 + z(\tau_0) - z(\tau) + [\dot{y}_0 + \dot{z}(\tau_0)](\tau - \tau_0), \tag{23}$$

$$\dot{y}(\tau) = \dot{y}_0 + \dot{z}(\tau_0) - \dot{z}(\tau) \tag{24}$$

and the condition for an impact is simply

$$y(\tau) = \pm \frac{v}{2}. \tag{25}$$

Just after the impact, the cart and particle variables are reset according to

$$\tau_0 = \tau, \quad y_0 = y(\tau), \quad z(\tau_0) = z(\tau), \tag{26–28}$$

$$\dot{y}_0 = -r\dot{y}(\tau), \quad \dot{z}(\tau_0) = \dot{z}(\tau) + \sigma(1 + r)\dot{y}. \tag{29, 30}$$

5. Control of chaotic impacts

The solutions of the dynamical equations (9) and (10) were obtained by numerical integration. We have been using the following numerical values for the parameters describing the cart motion: $\mu = 0.02$, $\delta = 0.1$, $\varepsilon = 0.1$, $E_1 = 2.5$, $E_2 = 1.5$. The particle motion, on their hand, is obtained

using the analytical solutions (14) and (15) or (23) and (24), in the absolute or relative reference frames, respectively, with parameters: $v = 12$ and $r = 0.7$. Once a collision has occurred, i.e., when either of conditions (16) or (25) holds, the variables are reset according to Eqs. (17)–(21) or (26)–(30), depending on what coordinate system we are using. In Ref. [17] preliminary results were shown, for a slightly different version of this system, showing a rich dynamical structure when the motor parameter E_1 is varied in the interval between 1.0 and 6.0, the displacement rate of the bouncing particle undergoing periodic as well as chaotic motion.

Let us consider the same physical setting as shown by Fig. 2 for the cart motion, with two coexisting chaotic attractors, and include now the effects of the impact dampers. In this case, the mass of the particle is much less than the total cart mass ($m/M \ll 1$). Fig. 4 shows the trajectories of the bouncing particle for both attractors, as a zig–zag motion bounded by a wiggling line representing the displacements of the walls, for the right-hand (Fig. 4(a)) and the left-hand (Fig. 4(b)) attractors. By using a reference frame moving with the cart, the wall positions are fixed and the particle motion is bounded, such that it can be represented in a phase space displacement versus velocity. Figs. 5(a) and (b) refer to the situation depicted in Figs. 4(a) and (b), respectively.

The transfer of momentum which follows each collision between the bouncing particle and the walls attached to the cart is responsible for an effective coupling so that the motion of the cart can

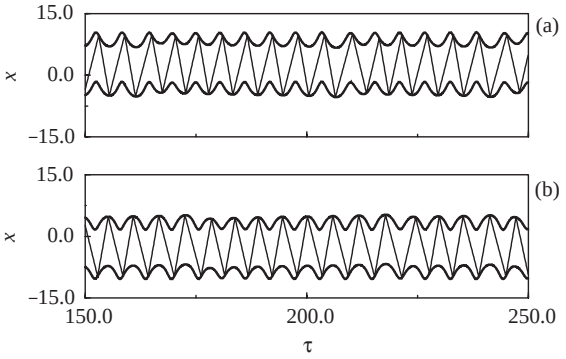

Fig. 4. Time series of the displacement x of the bouncing particle for the attractors (a) A, and (b) B of Fig. 2. The remaining parameters were $v = 12$, $r = 0.7$.

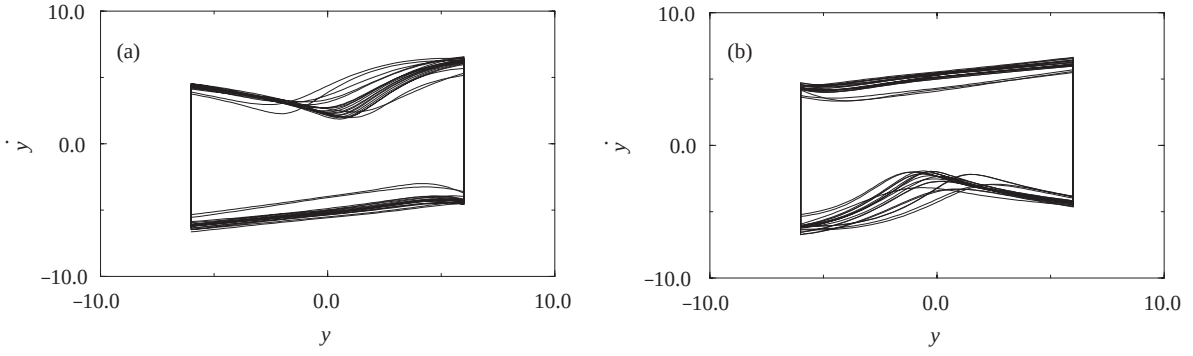

Fig. 5. Phase space (displacement versus velocity) of the bouncing particle in a reference frame moving with the cart for attractors (a) A, and (b) B of Fig. 2.

be controlled by the bouncing motion of the particle. The variable parameter, in this case, can be the ratio m/M between the masses of the cart and the bouncing particle. For small values of this ratio, we have essentially the same situation we discussed before: the coexistence of two chaotic attractors, symmetrically placed with respect to the $z = 0$ line. Fig. 6 shows a bifurcation diagram, in which the asymptotic motion of the cart is plotted against the mass ratio. In effect, for $m/M \approx 0.0045$ the chaotic motion is controlled, since the attractors now are stable periodic orbits.

Fig. 7(a) shows the phase space for the cart motion and $m/M = 0.005$, after the control has been achieved, and the formerly existent chaotic attractors, named as A and B, have been replaced

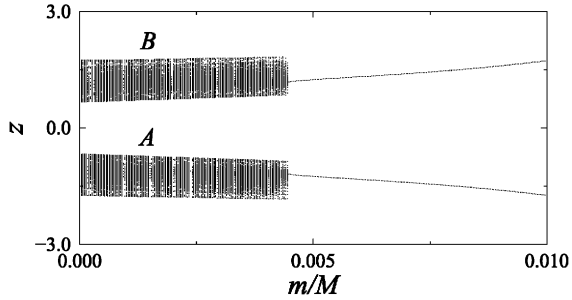

Fig. 6. Bifurcation diagram showing the attractors in the phase space of the cart motion, as a function of the particle–cart mass ratio m/M.

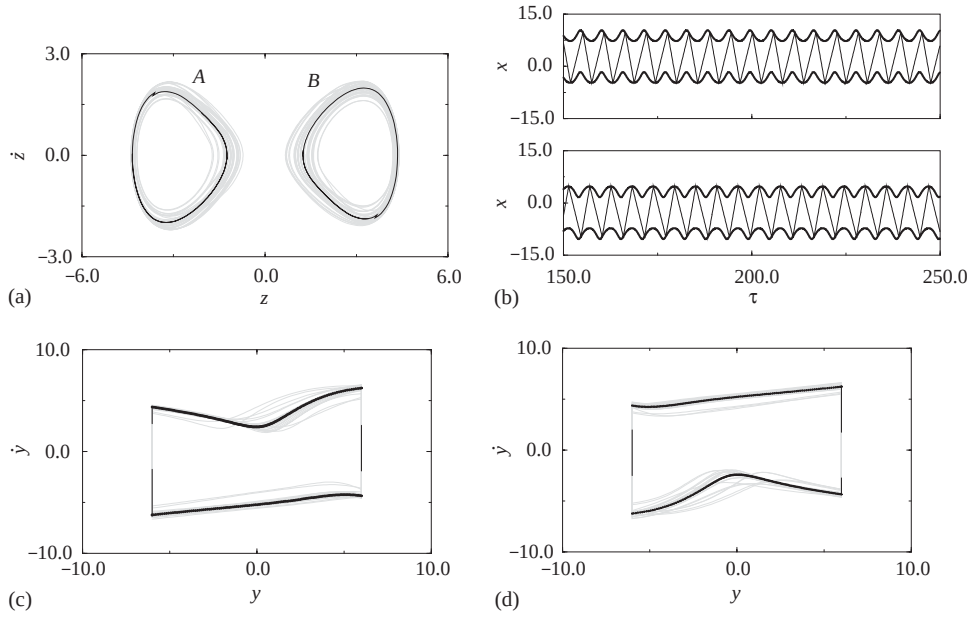

Fig. 7. (a) Displacement versus velocity of the cart for the same parameters of Fig. 2 and a bouncing particle of mass $m/M = 0.005$ showing two periodic orbits named as A and B embedded in the former chaotic attractors; (b) time series of the displacement x of the bouncing particle for the periodic orbits A and B; phase space (displacement versus velocity) of the bouncing particle in a reference frame moving with the cart for attractors (c) A, and (d) B, superimposed on the chaotic trajectories.

by two stable trajectories represented as bold curves superimposed on the chaotic attractors. This kind of stabilization resembles that achieved by the OGY technique for controlling chaos [22], and which was used in Ref. [23] to control unstable periodic orbits in mechanical systems with impacts.

Another effect of the coupling is that not only the cart but also the bouncing particle has a periodic motion. This can be observed in Fig. 7(b) for the two controlled periodic attractors of the cart motion. Figs. 7(c) and (d) refer to the same situation, but using a reference frame moving with the cart. The latter figures show the controlled motion superimposed to the uncontrolled chaotic oscillations of the bouncing particle.

The structure of the phase space of the cart motion, when we consider the motion of the bouncing particle, is very similar to that when there is no collisions, as can be shown in Fig. 8(a). A comparison with Fig. 2(b) reveals a similar structure of intertwined smooth and fractal basin boundary, with minor differences in the vicinity of the $z = 0$ symmetry line. In fact, taking into account the collisions is equivalent to breaking this symmetry. The time it takes for a trajectory starting at some initial condition to settle down into one of the two chaotic attractors (whose basins are depicted in Fig. 8(a)), can be measured in the number N of the impacts of the bouncing particle.

Fig. 8(b) shows a gray-scale representation of the number of transient impacts, in which the brighter (darker) the pixel, the less (more) is the number of collisions it takes for the trajectory to settle down in either of the chaotic attractors. As a general pattern, the farther is the initial condition from the region occupied by the attractors, the greater is the number of impacts

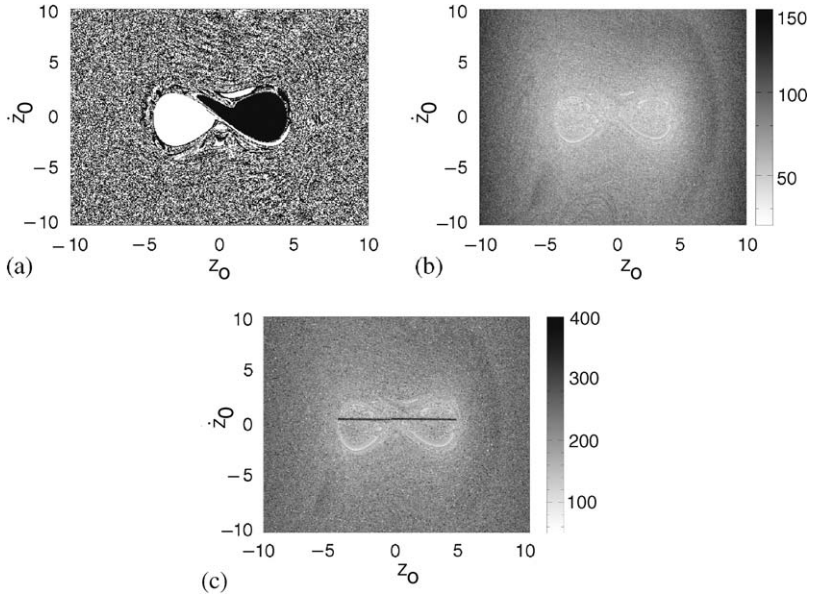

Fig. 8. (a) Basins of attraction of the orbits A (white region) and B (dark region) of Fig. 5; (b) number of impacts a given trajectory needs to settle down in either attractor represented in gray-scale, where the darker the pixel, the longer it takes; (c) same as (b), but considering the rescaled time. The initial conditions chosen were $\phi_0 = \dot{\phi}_0 = 0$, $y_0 = \tau_0 = 0$ and $\dot{y}_0 = -0.5$.

necessary. The regions comprised of initial conditions which generate transient motion with a given duration has been also called a *transient basin* [27].

In view of the incursive nature of the fractal striations present in the basin boundary diagram, there are channels through which the orbit is steered rapidly into the attractor. This is particularly clear in the white regions surrounding the lobes in Fig. 8(b). If we plot the transient time instead of the number of impacts, a similar picture is produced (Fig. 8(c)). The dark line at $\dot{z} \gtrsim 0$ shown in Fig. 8(c) and absent in Fig. 8(b) can be interpreted as follows: for low velocities (small $\dot{z}_0$) there are relatively few impacts, and the transient time increases since the momentum transfer is too small.

The interwoven basin structure observed in Fig. 8 suggests that the nature of the basin boundary is still a fractal one. In order to provide numerical evidence to support this conjecture, we picked up two boxes, Figs. 9(a) and (b), and computed the uncertain fraction for them. The results are plotted in Fig. 9(c) in terms of the radius ϖ of the uncertainty ball centered at each initial condition belonging to the boxes. The uncertainty exponents were found, up to the statistical accuracy, to be equal to $\alpha = 0.29 \pm 0.02$ for both boxes, which gives an estimative for the box-counting dimension of the basin boundary $d_B \approx 1.71$. Note that the uncertainty exponent in the model with impacts is 26% less than in the corresponding computation made without impacts, which leads to a correspondingly higher basin boundary dimension.

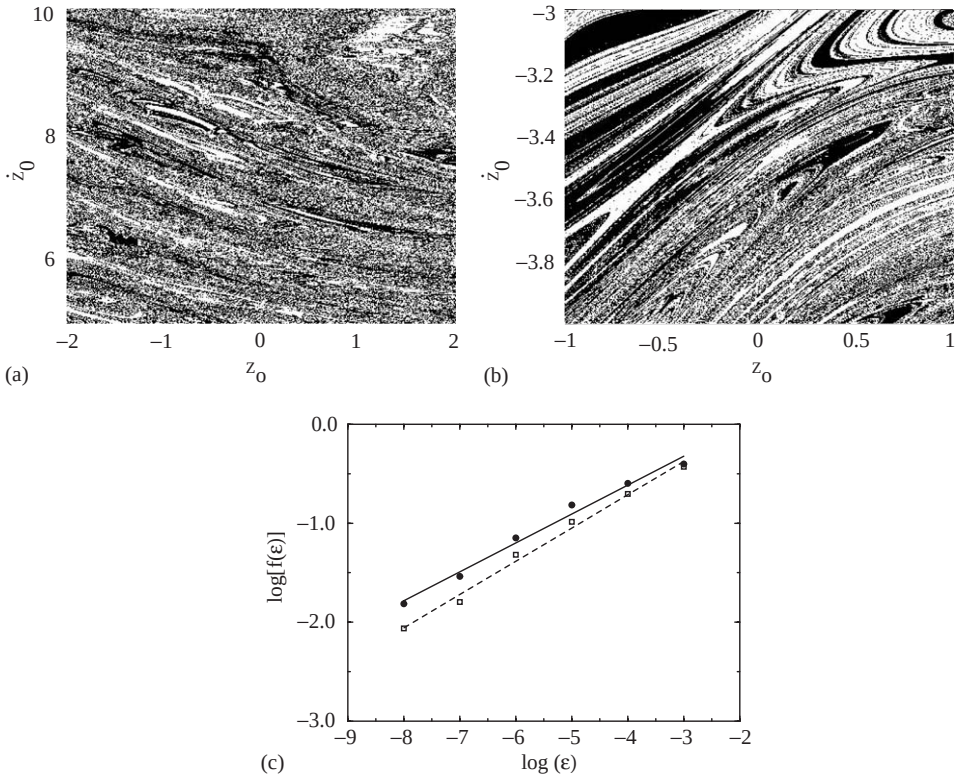

Fig. 9. (a,b) Two boxes picked up from Fig. 8(b) and which exhibits an apparently fractal basin structure; (c) uncertain fraction versus the radius of an uncertainty ball centered at an initial condition chosen from boxes (a) (filled circles) and (b) (open squares). The solid and dashed lines are least-squares fits, respectively.

6. Conclusions

The purpose of this paper was twofold: firstly to show numerically that the use of impact dampers is efficient to control chaotic oscillations of a non-ideal system modelled by a cart endowed with a rotor with a limited energy supply. In fact, we have obtained a suppression of chaotic motion with a very small ratio (about 0.5%) between the masses of the cart and the bouncing particle. From the technical point of view, the smaller this ratio, the easier it is to install such impact dampers in engineering systems like turbine blades and cutting tools. Previous studies [6] have pointed out higher values for this ratio, but in our work we show that it can be considerably lowered due to the non-ideal character of the forcing (a consequence of its limited energy supply).

The second goal we have set up for this paper was to explore numerically the highly interwoven structure of the phase space for this system. In practical terms, the more intertwined the attraction basins are, the more difficult is to predict to what stationary state will the system be attracted to for long times. Our results suggest that, instead of turning the phase space smoother, the addition of an impact damper, even though having an effect of controlling chaos, has also the undesirable effect of increasing the final-state sensitivity in the phase space and turning the dynamical system even less predictable than before. This may be a serious problem if one of the attractors would correspond to an undesired behavior and one is interested to avoid the system to asymptote to such a state. In this case, one has to be very careful and choose the initial conditions with an uncertainty as low as possible.

Acknowledgements

This work was made possible by partial financial support from the following Brazilian government agencies: FAPESP, CAPES, CNPq and Fundação Araucária.

References

[1] J.M.T. Thompson, H.B. Stewart, *Nonlinear Dynamics and Chaos*, Wiley, Chichester, 1986.
[2] F.C. Moon, *Applied Dynamics with Applications to Multi-body and Mechatronic Systems*, Wiley, New York, 1998.
[3] T. Kapitaniak, *Chaos for Engineers*, Springer, Berlin, 2000.
[4] B. Blazejczyk-Okolewska, K. Czolczynski, T. Kapitaniak, J. Wojewoda, *Chaotic Mechanics in Systems with Friction and Impacts*, World Scientific, Singapore, 1999.
[5] M. Wiercigroch, B. Dekraker, *Applied Nonlinear Dynamics and Chaos of Mechanical Systems with Discontinuities*, World Scientific, Singapore, 2000.
[6] S. Chaterjee, A.K. Mallik, A. Ghosh, On impact dampers for non-linear vibration systems, *Journal of Sound and Vibration* 187 (1995) 403–420.
[7] S. Chaterjee, A.K. Mallik, A. Ghosh, Impact dampers for controlling self-excited oscillation, *Journal of Sound and Vibration* 193 (1995) 1003–1014.
[8] A.L. Paget, Vibration in steam turbine buckets and damping by impacts, *Engineering* 143 (1937) 305–307.
[9] M.M. Sadek, Impact dampers for controlling vibration in machine tools, *Machinery* 120 (1972) 152–161.
[10] H.H. Reed, Hanging chain impact dampers—a simple model of damping tall, flexible structures, *Wind Effects on Buildings and Structures*, *Proceedings of Internal Research Seminar*, Ottawa, 1967.

[11] A.B. Nordmark, Non-periodic motion caused by grazing in an impact oscillator, *Journal of Sound and Vibration* 145 (1991) 279–297.
[12] K. Karagiannis, F. Pfeiffer, Theoretical and experimental investigations of gear-rattling, *Nonlinear Dynamics* 2 (1991) 367–387.
[13] H. Dankowicz, P. Piiroinen, Exploiting discontinuites for stabilization of recurrent motions, *Dynamical Systems* 17 (2002) 317–342.
[14] J. Warminski, J.M. Balthazar, R.M.L.R.F. Brasil, Vibrations of a non-ideal parametrically and self-excited model, *Journal Sound and Vibration* 245 (2001) 363–374.
[15] V.O. Kononenko, *Vibrating Systems with a Limited Power Supply*, Iliffe Books, London, 1969.
[16] T.S. Krasnopolskaya, A.Y. Shvets, Chaos in vibrating systems with a limited power-supply, *Chaos* 3 (1993) 387–395.
[17] S.L.T. de Souza, I.L. Caldas, J.M. Balthazar, R.M.L.R.F. Brasil, Analysis of regular and irregular dynamics of a non ideal gear rattling problem, *Journal of the Brazilian Society of Mechanical Sciences* 24 (2002) 111–114.
[18] F.C. Moon, G.X. Li, Fractal basin boundaries and homoclinic orbits for periodic motion in a two-well potential, *Physical Review Letters* 55 (1985) 1439–1442.
[19] L.D. Zavodney, A.H. Nayfeh, N.E. Sanchez, Bifurcations and chaos in parametrically excited single-degree-of-freedom systems, *Nonlinear Dynamics* 1 (1990) 1–21.
[20] S.W. McDonald, C. Grebogi, E. Ott, Fractal basin boundaries, *Physica D* 17 (1985) 125–153.
[21] S.W. McDonald, C. Grebogi, E. Ott, Final state sensitivity: an obstruction to predictability, *Physics Letters A* 99 (1983) 415–418.
[22] E. Ott, C. Grebogi, J.A. Yorke, Controlling chaos, *Physical Review Letters* 64 (1990) 1196–1199.
[23] S.L.T. de Souza, I.L. Caldas, Controlling chaotic orbits in mechanical systems with impacts, *Chaos, Solitons and Fractals* 19 (2004) 171–178.
[24] J.P. Eckmann, D. Ruelle, Ergodic theory of chaos, *Reviews of Modern Physics* 57 (1985) 617–656.
[25] C. Grebogi, E. Kostelich, E. Ott, J.A. Yorke, Multi-dimensioned intertwined basin boundaries and the kicked double rotor, *Physics Letters A* 118 (1986) 448–452.
[26] S.L.T. de Souza, I.L. Caldas, Basins of attraction and transient chaos in a gear-rattling model, *Journal of Vibration and Control* 7 (2001) 849–862.
[27] M. Woltering, M. Markus, Riddled-like basins of transient chaos, *Physical Review Letters* 84 (2000) 630–633.